Chapter 1

Introduction

1.1 Overview

Organic electronics, such as organic light-emitting diodes (OLEDs), organic thin-film transistors (OTFTs), and organic solar cells and so on, have become one of the popular novel studies around the world over the last decade due to its low cost of fabrication and flexible properties. Various organic semiconducting materials have been used to fabricate OTFTs.

Organic semiconductors have been studied since late 1940s [1]. However, their semiconducting characteristics were poor and the devices were lake of reproducibility, which made these ill-defined materials impossible to be used in any real electronic devices. After a decade of intense research, both in universities and in private enterprises results showed the fact that organic semiconductors suffer from severe limitations, which is probably due to the existence of very high density of defects and traps, as well as to a very low carrier mobility [2]. The interests of organic-based semiconductors faded until the late 1970s, when a new class of materials was proposed in the literature. The prototype is polyacetylene [2]. These polymers were shown to exist in two states, one oxidized, possessing an intrinsic electrical conductivity, and the second neutral, with a less defined electrical behavior, ranging from insulating to semiconducting. The very high instability of polyacetylene under air restricted its characterization, and work was focused mainly on the electrical behavior of its oxidized state. The first FET sample fabricated by polyacetylene was reported in 1983, and due to its instability, the mobility was very low, on the order of 10^{-5} $cm^2V^{-1}s^{-1}$ [3]. Later on, air stable organic semiconducting material such as polythiophene and polyphenylenevinylene, PPV, could be electrochemically synthesized as thin films as the active layers. However, the

mobility was still lower than 10^{-4} $cm^2V^{-1}s^{-1}$. The first OTFT made of small conjugated molecules was demonstrated in 1989 [4]. The material was sexithiophene, which is an oligomer of polythiophene, made of six thiophene rings linked at the alpha position (Fig. 1-1a). The mobility was improved to 10^{-1} $cm^2V^{-1}s^{-1}$, almost can be comparable to that of amorphous hydrogenated silicon (a-Si:H).

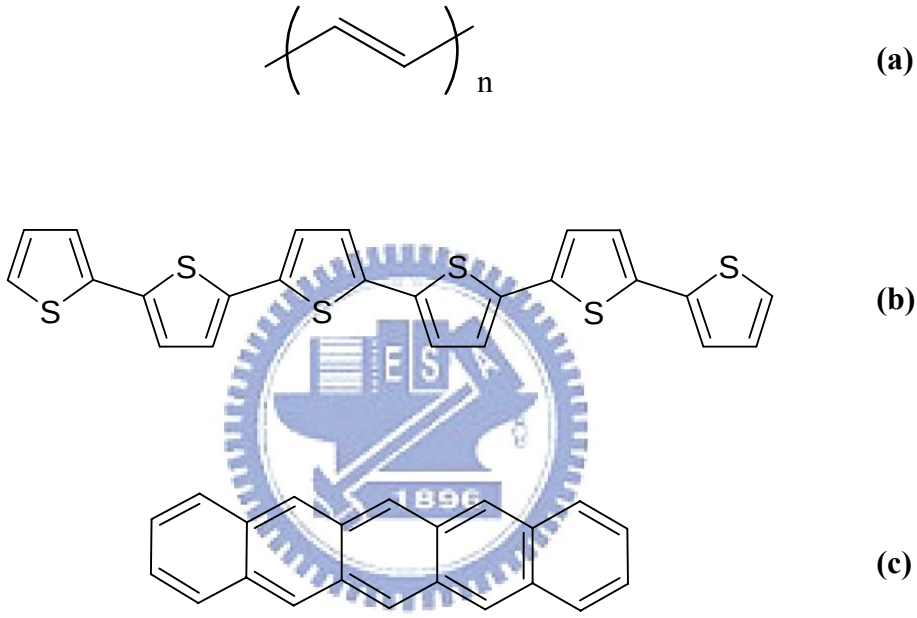

(a)

(b)

(c)

Fig. 1-1 Molecular structures of (a) polyacetylene (b) α-sexithiophene and (c) pentacene

So far, one of the most popular organic semiconducting materials is pentacene, which belongs to the family of polyacenes (Fig. 1-1b), which belongs to the family of polyacenes. Generally speaking, the pentacene thin film is often deposited by vacuum evaporation for realizing organic-based FETs. In early stage of the development of pentacene-based FETs, the value of mobility obtained was on the order of 2×10^{-3} $cm^2V^{-1}s^{-1}$ [5]. Recently, the mobility has been improved progressively to a benchmark value, which is higher than 1 $cm^2V^{-1}s^{-1}$ [6-9]

and is comparable to a-Si. The highest value reported to date is even as high as to 7 $cm^2V^{-1}s^{-1}$ [10]. Therefore, pentacene is the most promising organic semiconducting material for realizing commercial OTFT products in the future. In this thesis, we adopt pentacene as the model compound for its milestone mobility.

1.2 The Basic Device Structure

1.2.1 Pentacene

One of the most important factors to affect the mobility is the morphology of organic semiconducting materials. Pentacene exhibits a strong tendency to form highly ordered films. However, the morphology depends strongly on the growth conditions, purity, and the types of substrate surface. On the other hand, bulk single crystals are not favorable for low cost electronics, because the fabrication is time consuming and the crystals are small. Thin films are usually more favorable, because they can be fabricated on various substrates. The hole mobility of thin film pentacene is close to the intrinsic transportation limit of bulk single crystal. The TFTs made of pentacene also has mobility of larger than 1 $cm^2 V^{-1}s^{-1}$ [11-13].

Carrier transport is easiest parallel to the π-conjugation direction, thus this direction should be parallel to the gate insulator surface in organic TFTs, which means that each molecule should be positioned with its long molecular axis almost perpendicular to this surface. Fig. 1-2 contains proof of the foregoing claims. By growing amorphous films of pentacene, which is achieved by keeping the substrate temperature at -196 ^oC during deposition. The resulting film exhibits a typical insulating behavior. The overlap of the molecular orbitals of nearest-neighbor molecules is very limited because of the disorder in the solid. When the substrate temperature is kept at room temperature (27 ^oC) during deposition, a highly ordered film is obtain and the device mobility measured at room temperature is 0.6 $cm^2V^{-1}s^{-1}$ [14]. The well-defined X-ray diffraction peaks, corresponding to (00l) reflections,

with a d-spacing of about 15.4 Å, corresponds to a crystalline structure with the long axis of the pentacene molecule being almost perpendicular to the substrate surface. The structure of this thin film is different from the structure of single crystals of pentacene; thus we must distinguish between the “thin-film phase” [6] and “single crystal phase” [15]. One of the main differences between these phases is in the d-spacing of the (00l) reflections. It is slightly smaller (14.5 Å) in the “single crystal phase”; thus in this phase the long axis of the pentacene molecule has a larger angle with respect to the substrate surface normal than that in the “thin-film phase.” When a mixture of the thin-film phase and the single-crystal phase is grown at higher deposition temperatures, the mobility is very low, possibly due to the high defect concentration resulting from the coexistence of the two phases [16]. Obviously, the deposition rate also influence on the thin-film morphology deeply. Hence, both parameters (temperature and deposition rate) have to be controlled accurately when trying to produce a specific morphology.

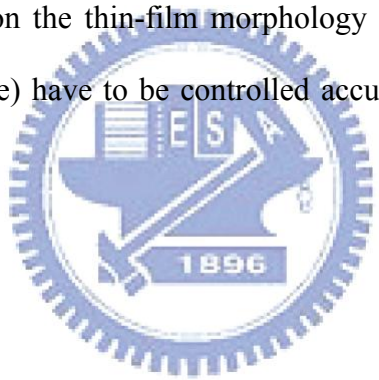

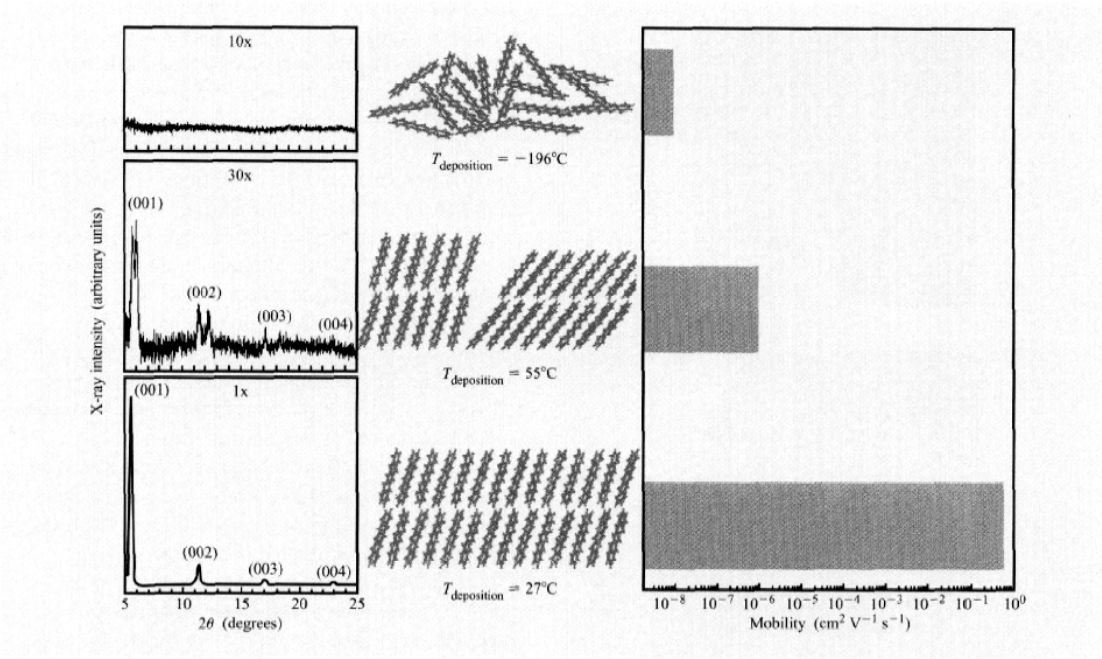

Fig. 1-2 Comparison of X-ray diffraction pattern, schematic representations of structural order, and field-effect mobilities for three different phases of thin film pentacene. An amorphous phase is achieved using a substrate temperature, $T_{deposition}$, of -196 ^{o}C and a deposition rate DR of 0.5 Ås^{-1}, A single phase results at the temperature $T_{deposition}$ = 27 ^{o}C and DR =1 Ås^{-1}, while $T_{depeposition}$ = 55 ^{o}C and DR = 0.25 Å s^{-1} yields a double phase. (Reprinted from Ref. [14])

1.2.2 Inverted-Coplanar and Inverted-Staggered Organic TFT

The inverted-coplanar OTFTs (bottom-contact OTFTs) and inverted-staggered organic TFT (top-contact OTFTs) are the two most common kinds of organic FETs so far. However, the devices characteristics are different. The most studies, so far, are focused on top contact configuration, in which the source/drain contacts are patterned by shadow masking on top of

the organic semiconductor such as pentacene, because of its better and stable performance (Fig. 1-3a). Unfortunately, this process cannot be used in mass production; that a protocol that was allowed the patterning of the source and drain electrodes on the insulator before the deposition of pentacene (Fig. 1-3b). This fabrication process can operate in coordination to common semiconductor process with ultra-short channel length and fine electrode patterns by the photolithograph technology. Larger throughput is also one of the benefits.

However, the pentacene layer which was grown on SiO_2 (bottom part of Fig. 1-4) is much different from that on a Au electrode (upper part of Fig. 1-4) [17-18]. The pentacene on SiO_2 far away from the Au edge consists of fairly large grains (having sizes, between 0.2 and 0.5 μm, as shown in bottom photograph of Fig. 1-4). On Au the grain size is dramatically reduced (top photograph of Fig. 1-4). This small crystal growth persists into the channel region (on SiO_2) [17-18]. Close to the Au edge, but on the SiO_2 side, there is a transition region where the grain size increases with increasing distance from the edge (middle photograph). It is the morphology of the pentacene film in the OTFT channel region close to the electrode edge that causes the performance limitation of the bottom contact TFTs. Right at the edge of the Au electrode, there is an area with very small crystals and thus a large number of grain boundaries. Grain boundaries are high-volume and low-order regions that contain many morphological defects, which in turn are linked to the creation of charge carrier traps lying in the band gap. The creation of an unusually large concentration of defects in the region of the channel close to the electrode edge can be considered responsible for the reduced performance of bottom contact pentacene TFTs. The reduction of the concentration of defects near electrodes (lower part of Fig. 1-4) should result in bottom contact devices with performance similar to or better than that of top contact devices

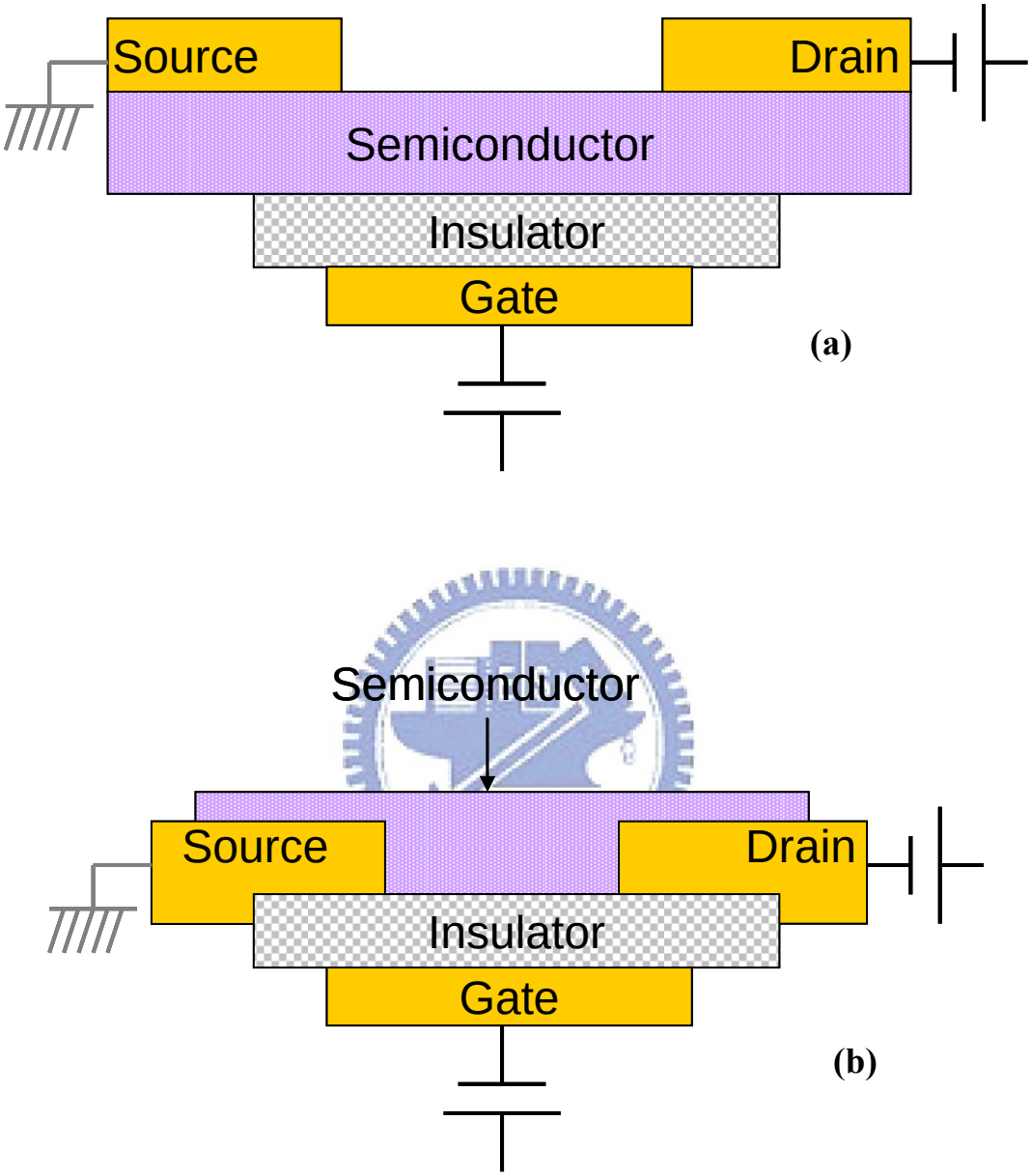

Fig. 1-3 General OTFT device configurations. (a) Top contact device and (b) Bottom-contact device

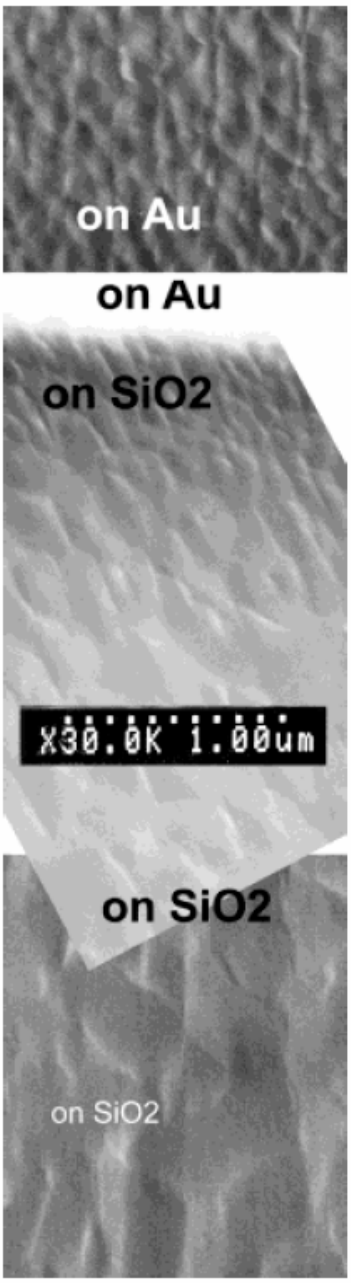

Fig. 1-4 Scanning electron microscopy (SEM) image of a pentacene thin film grown on SiO_2 and a Au electrode. The grain size is much smaller on Au than that on SiO_2 far from the Au edge. The pentacene grain size on SiO_2 in the region close to the Au edge is similar to that on Au and increases with increasing distance from the edge. (Reprinted from [17])

1.3 Contact Resistance

1.3.1 Introduction

The CuPc modification electrode for improving carrier injection efficiency is the focus in this thesis. Therefore, we will emphasize on the extraction of contact resistance and on demonstrating improved performance. The decrease of contact resistance should give a direct evidence of improvement of injection efficiency. However the estimation of contact resistance for organic TFT is not as easy as that for inorganic TFT made of silicon. The source and drain contacts in organic are not easily optimized by conventional processes, such as semiconductor doping or metal alloying.

1.3.2 The Extraction of Contact Resistance [19, 20]

The parasitic resistance can be extracted form the current-voltage characteristics of the devices with different channel lengths. In the linear regime, the overall device resistance R_{on} can be written as the sum of the intrinsic channel resistance R_{ch} and the parasitic resistance R_p according to

$$R_{on} = \frac{\partial V_{DS}}{\partial I_{DS}}\Big|_{V_{ds}\to 0}^{V_g} = R_{ch} + R_p = \frac{L}{W\mu_i C_i (V_G - V_{T,i})} + R_p \qquad (1\text{-}1)$$

where μ_i and $V_{T,i}$ are the intrinsic mobility and threshold voltage, respectively. In the linear regime of I_D-V_G curve, the transfer line is close to linear relation and follows the Ohmic's theory. The total resistance R_T comprises two elements, the contact resistance and the channel resistance. The contact resistance is the one between the electrode and organic channel, showed in Fig. 1-5. The channel resistance is the one of the field-effect channel adjoins the organic/insulator interface and, consequently, depends on the bias of the gate electrode. Plotting the corresponding resistance as a function of channel length leads to straight line, the slope of which is proportional to the channel resistance, while the contact resistance is given

by the extrapolation of the line to zero length (Eq. 1-1). Thus, we can calculate the contact resistance by finding the intersect of the approximation line with Y-axis. (Fig. 1-6)

By considering the requirement of larger current output, the short channel OTFT devices will be the main stream in the near future. From the literature, it has been shown that the contact resistance was a substantial part of the total TFT resistance especially for relatively short channel (L < 15 μm) OTFTs. (Fig. 1-7) To reduce the contact resistance must be one of the important concerns to improve the performance of OTFTs.

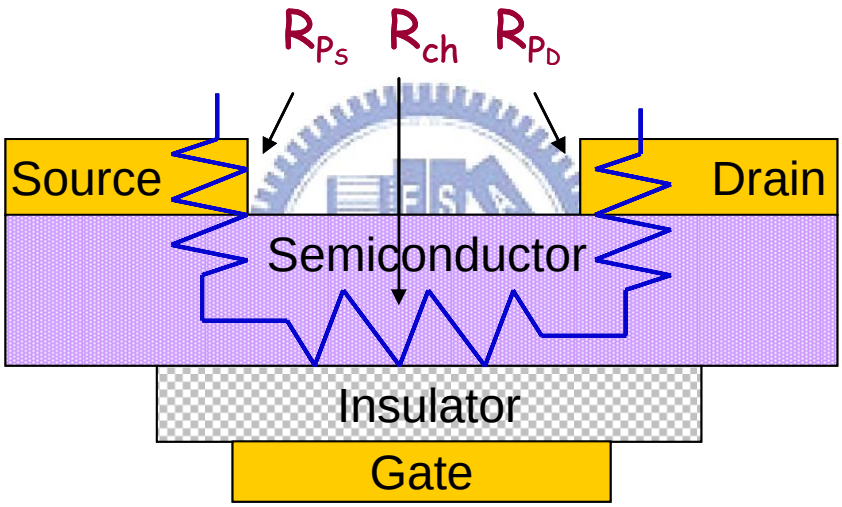

Fig. 1-5 The illustrations shows the channel resistance (R_{ch}) and the contact resistance (R_P).

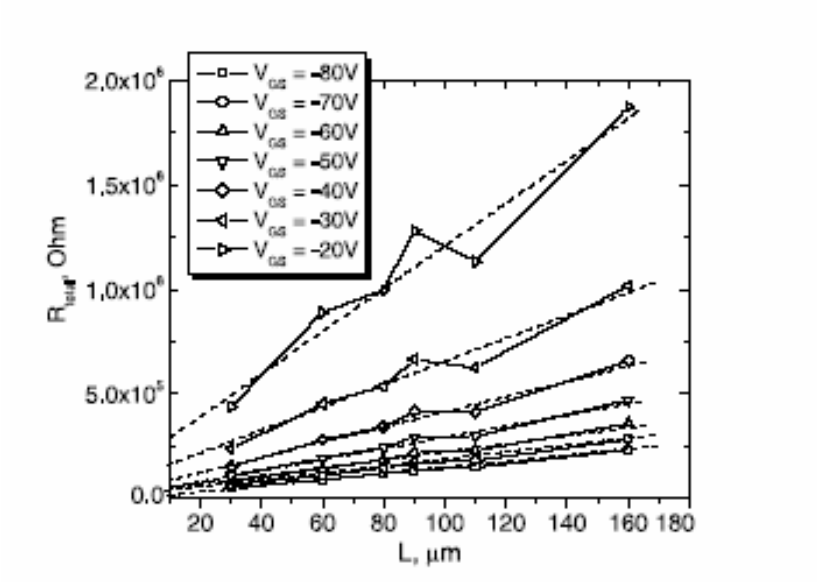

Fig. 1-6 Gold TC TFTs (*W*= 1200µm) total resistance at different V_{GS} as a function of *L*. (Reprint from [20])

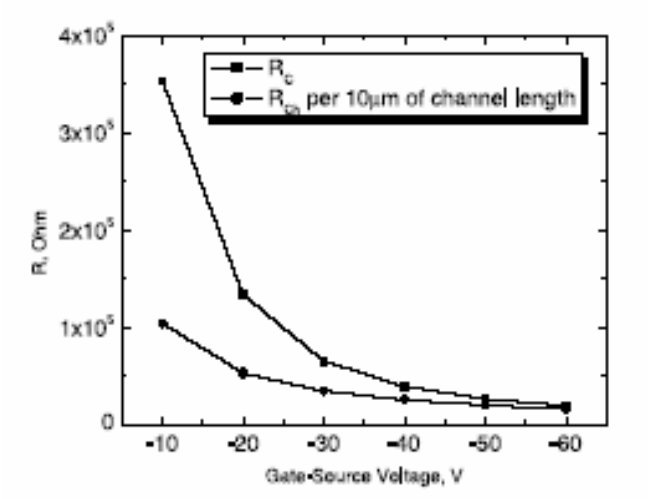

Fig. 1-7 Extracted gold TC TFTs contact resistance (R_C) and channel resistance (R_{Ch}) per 10 µm of the channel length (W= 1200µm) (Reprint from [20])

1.4 Motivation

There are many unclear and unidentified mechanisms need to be studied for pentacene-based TFTs. Such as the definition of field effect mobility behaviors and environment influence, all need be further considered. However, not only the fundamental characteristics of OTFTs we will concentrate on, but the improvement of the organic TFTs for wider usage should be taken into consideration. Because of the low mobility and high threshold voltage of OTFTs, the operation voltage was usually as high as 100 Volts for high current output or complete and better current/voltage characteristics. But it is not grand for a common electrical circuit operated at such high bias; therefore, it is needed to look for some methods to solve these serious problems.

1.5 Organization

This thesis is organized as follows. In **Chapter 2**, the details of energy diagram involved in OTFTs are described. Finally, the idea of enhancement of charge injection is deduced. In **Chapter 3**, OTFT fabrication flows and data analysis are presented. Moreover, we propose a pentacene-based diode for demonstrating the enhancement of charge injection. In **Chapter 4**, we summarize all the experiment results briefly.

Chapter 2

The Transportation Mechanism and Characteristics of Organic Thin Film Transistors

2.1 Introduction

2.1.1 Interfaces in Organic Electronics

Recently the energy diagram of electronically functional organic materials has attracted much interest for various applications. In many cases, the function originates from the interfaces. Some examples are shown in Fig. 2-1 with schematic energy diagrams: Fig. 2-1(a) shows an organic electroluminescent (EL) device in which electrons (e^-) and holes (h^+) are injected from the electrodes into electron transport layer (ETL) and hole transport layer (HTL), respectively. These carriers recombine to emit light, possibly in another emission layer [21, 22]. Fig. 2-1(b) depicts spectral sensitization in silver halide photography. In this process, an electron is photo-excited in an organic dye molecule adsorbed on an silver halide (AgX) surface, and is injected into the conduction band of AgX, leading to sensitization [23]. Fig. 2-1(c)shows an organic solar cell: Photo-formed electron-hole pairs in the organic layer are separated in the bent band region accompanied by the Schottky barrier.[24] Thus the elucidation of the interfacial electronic structure forms the basis for understanding and improving the performance of these devices. In particular, the organic/metal and organic/organic interfaces have attracted much interest in relationship between the rapid development of the organic EL and FET devices.

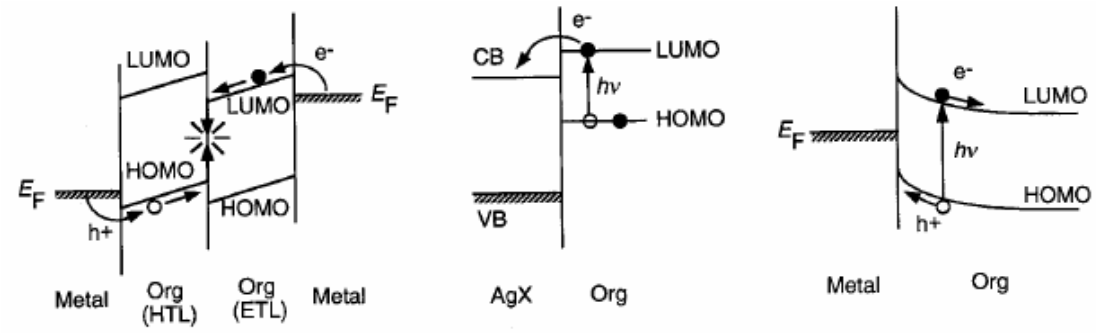

(a) (b) (c)

Fig. 2-1 Energy diagrams of organic electronic devices with functions originating at interfaces. (a) EL device. (b) Spectral sensitization in silver halide photography. (c) Organic solar cell using metal/organic Schottky barrier. (Reprinted from [25])

2.1.2 The Carrier Transportation in Organic Semiconductors

Van der waals force is the only binding energy between organic semiconductor molecules with energy smaller than 10 Kcal mol^{-1}. This weak interaction energy of molecules may take responsibility for the low upper limit of carrier mobilities, falls between 1-10 $cm^2V^{-1}s^{-1}$ by time-of-flight measurement [26], due to its value close to the vibration energy of molecules. Whereas in inorganic semiconductors that are joined by covalent bonds, the intermolecular bonding energy is as strong as 76 Kcal mol^{-1} in silicon. Thus the carriers move as highly delocalized plane waves in wide band with high mobility.

The conjugated organic materials containing the specific π electron orbitals that make the carriers possible to move between molecular. In well-order organic semiconductors, the energy of excitation state and the steady states of π electron would extend and split to form a band-like energy scheme. The energy scheme is similar to that in inorganic semiconductor

(see **Chapter 2.3** for detail), where the lowest unoccupied molecular orbital (LUMO) like the conduction band and the highest occupied molecular orbital (HOMO) as the valence band (see Fig. 2-2d or 2-2e), The band-like energy structure make the carrier transport more close to the behavior in inorganic semiconductors.

However, band transport maybe not suitable for disordered organic semiconductors, in which carrier transport is dominated by hopping between localized states. It is thermally activated process, which is assisted by phonons. The mobility increases with the increasing temperature, although the overall mobility remains comparative low, usually much lower than 1 $cm^2V^{-1}s^{-1}$. However, the mobility of the organic semiconductor film is as high as 1 $cm^2V^{-1}s^{-1}$ by band-like transport at room temperature. Many kinds of polycrystalline organic semiconductors like acene series, pentacene, rubrene, have mobility falling in the range. Sometimes, a temperature-independent mobility was found in some polycrystalline pentacene film [27]. The observation argued that the simply thermal activated hopping process dominated the whole carrier transporting behaviors in the high quality polycrystalline pentacene film, despite that the defects enhanced film quality may cause mobility increase with temperature in some cases.

The understandings of carrier transport in a single crystalline organic semiconductor help us to understand the transporting mechanism in a polycrystalline organic semiconductor film. It was believed that the carrier transport mechanism in single crystal is coherent band-like transport of delocalized states at low temperature. A high mobility for holes, 400 $cm^2V^{-1}s^{-1}$, measured by time-of-flight in single crystal naphthalene at 4.2 K was observed [28, 29]. The hole mobility which follows a power low of $\mu \propto T^{-n}$, n = 2.79, increases from 1 $cm^2/V^{-1}s^{-1}$ at room temperature to 400 $cm^2V^{-1}s^{-1}$ at 10 K. This is a clear evidence of band transport in single crystalline organic semiconductors. On the other hand, the electron mobility was also found temperature-dependent below 100 K and following the power law of $\mu \propto T^{-n}$, n ~ 1.5-1.7, in single crystal naphthalene [28, 30, 31]. However, between 100 K and 300 K, the electron

mobility revealed a constant value [31, 32], that has been treated as the superposition of two independent carrier transport mechanism. And this mechanism was thought as the tunneling of small molecular polaron (MP), that the carriers were treated as heavy polaron type qusiparticles formed by interaction between carriers with intra-molecular vibrations of the local lattice environment. In this model, the mobility followed the power law of $\mu_{MP} \propto \alpha T^{-n}$.Another one is the moving of small lattice polaron (LP) by thermal activated hopping, which followed an exponential dependence with temperature of $\mu_{LP} \propto \exp[-E_a / kT]$. The superposition of these two mechanisms could explain the experiment data well from room temperature to a few Kelvin degrees [31].

It is very important to realize the carrier transport mechanism for organic electrical devices. Although the ultrapure organic semiconductors demonstrated a coherent band-like transportation, the most real organic semiconductor films with polycrystalline contained many structure defects, such as grain boundaries. Those defects dominated the carrier transport though affecting the energy barrier height in grain boundaries.

Based on the concept mentioned above in general, there are two methods to enhance the carrier transport, or mobility, in organic semiconductors. One is to strength the intermolecular force in organic semiconductor to form a more rigid structure that would enhance the transport of delocalized carriers by lattice vibrations (phonons). Another is to build a structure that carrier transporting only through intramolecular. That could be realized by long chain polymers or a very short channel length. However, both of them are not easy for mass production.

2.2 The Basic Operation Mode of Organic Thin Film Transistors

The OTFTs are adequately modeled by standard field-effect transistor equations [32], as shown previously for other organic TFTs [33, 34]. The pentacene used in the present study behaves as a ***p***-type semiconductor. A typical plot of drain current, I_D, vs. drain voltage, V_D, at various gate voltages, V_G, is shown in Fig. 2-2. The pentacene layer in this device was deposited at room temperature. When the gate electrode is biased negatively with respect to the source electrode (grounded), pentacene OTFTs operate in the accumulation mode and the accumulated charge are holes. At low V_D, I_D increases linearly with V_D (linear regime) and is approximately given by the Eq. 2-1

$$I_D = \frac{WC_i}{L}\mu(V_G - V_T - \frac{V_D}{2})V_D \qquad (2\text{-}1)$$

where L is the channel length, W is the channel width, C_i is the capacitance per unit area of the insulating layer (2000 Å thermally grown SiO_2 with C_i = 1.73 × 10^{-8} F/cm^2), V_T is the threshold voltage, and μ is the field-effect mobility. The mobility μ can be calculated in the linear regime in the following ways. First, it can be calculated from the transconductance

$$g_m = (\frac{\partial I_D}{\partial V_G})_{V_D=const} = \frac{WC_i}{L}\mu V_D \qquad (2\text{-}2)$$

By plotting I_D vs. V_G at a constant low V_D and equating the value of the slop of this plot to the transconductance.

Second, μ may be calculated by determining the slope $[(\partial I_D / \partial V_D)_{V_G=const}]$ in the linear regime of the I_D vs. V_D curve at various V_G. Then by plotting these slopes vs. V_G, and by

equating the slope of this plot $(\partial / \partial V_G)[(\partial I_D / \partial V_D)_{V_G=const}]_{V_D=const}$ to *(WCi/L)* μ, the mobility is the linear region can be obtained. For $\boldsymbol{V_D}$ greater than $\boldsymbol{V_G}$, $\boldsymbol{I_D}$ tends to be saturate (saturation regime) due to the pinch-off in the accumulation region. The behavior is modeled by the equation

$$I_D = \frac{WCi}{2L}\mu(V_G - V_T)^2 \qquad (2\text{-}3)$$

In the saturation regime, $\boldsymbol{\mu}$ can be calculated from the slope of the plot of $|\boldsymbol{I_D}|^{1/2}$ vs. $\boldsymbol{V_G}$

$$g_m = \left(\frac{\partial(-I_D)^{1/2}}{\partial V_G}\right)_{V_D=const} = \frac{WC_i}{2L}\mu \quad \text{(plotted in Fig. 2-3).} \qquad (2\text{-}4)$$

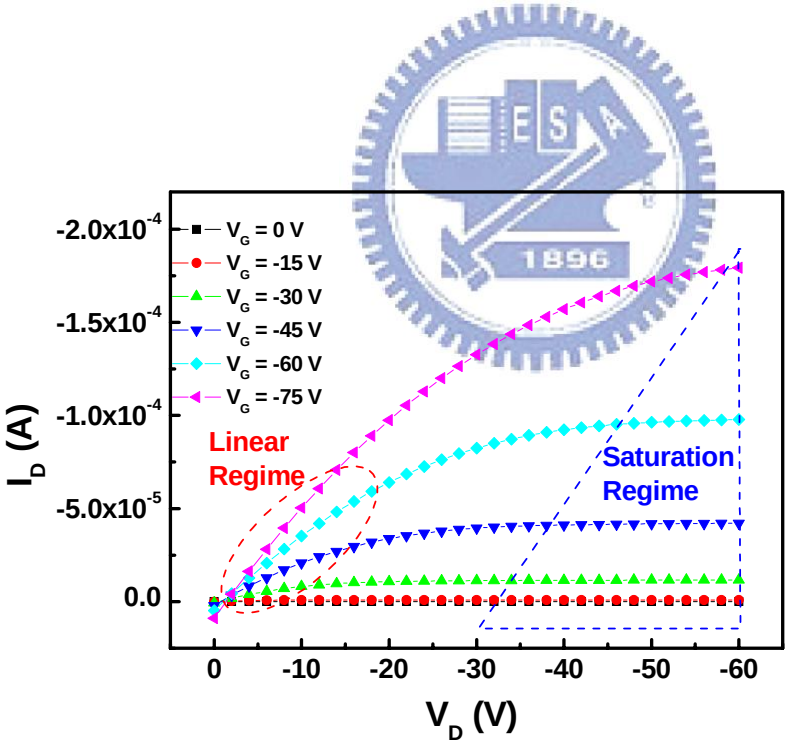

Fig. 2-2 Plot of drain current vs. drain voltage at various gate voltage values, from pentacene-based OTFTs.

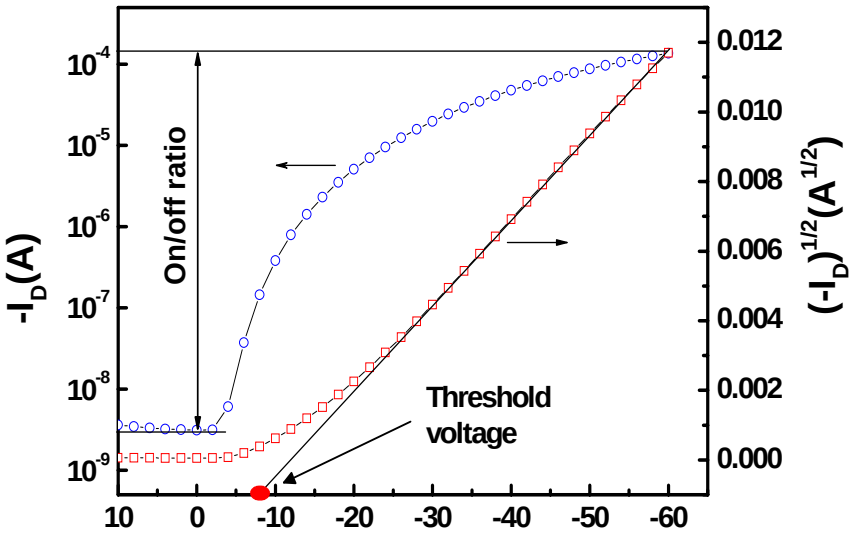

Fig. 2-3 Plot of drain current (left, y axis) and the square root of drain current (right, y axis) vs. gate voltage at a constant drain voltage of -60 V (saturation regime) from the same device as in Fig. 2-2.

2.3 The Critical Issue at Real OTFT Device

2.3.1 Introduction

Recent experimental and theoretical studies have suggested the presence of a significant interface dipole at the metal-organic interface [24]. This surface-dipole contribution is always substantially modified by the presence of an adsorbate. In the case of large adsorbates, such as conjugated organic molecules, the repulsion between the molecule electrons and the metal surface electrons leads to a compression of the electron tail leading to a lowering of the metal work function for the metal. This, in turn, causes an abrupt downward shift of the vacuum level from the metal to the organic film at the interface, i.e., a surface dipole barrier. The consequence of this systematic lowering of the metal Φ is a downward shift of the molecular energy levels and an increase in the energy difference between the metal Fermi level and the HOMO of the organic film. The interface between gold and pentacene has been studied by ultraviolet photoemission spectroscopy (UPS) [35]. The results indicate the presence of an interface dipole at the interface (Fig. 2-4), which leads to a relative large hole injection barrier (~1.0 eV) from Au to pentacene.

.

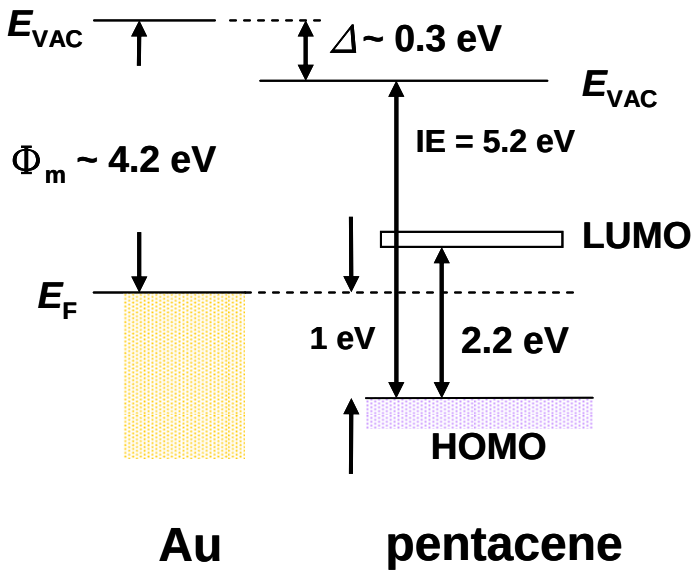

Fig. 2-4 Schematic energy level diagrams of the interfaces between the pentacene and Au, showing the Fermi level E_F, HOMO and LUMO, the vacuum level (E_{vac}) and ionization energy (IE), and the interface dipole Δ. (Replot from [36])

2.3.2 The Energy Diagram of Metal/CuPC

Fig. 2-5 illustrates the changes that occur as further Au is deposited onto the CuPc after 1 Å of Au has already been deposited [37]. We show the difference between the 1 Å of Au on CuPc and the subsequent depositions of Au. A feature located at 1.28 eV is seen to appear and grow as more Au is deposited. Another, smaller, feature at 2.9 eV is also seen to develop. The feature at 1.28 eV is a gap state that is induced by the donation of an electron from the CuPc to the Au. The feature that is seen at 2.9 eV is the result of the peak originally at 3.9 eV shifting toward the Fermi level as Au is deposited. By comparing a IPES spectrum from a bulk Au, as seen in the inset of Fig 2-5, to the difference spectra sample the Au does not exhibit any features in the range of interest, ensuring that the changes in the IPES spectrum is due solely to changes in the CuPc energy levels.

The appearance of a gap state between the HOMO and the Fermi level coupled with a

uniform shift of the other energy levels of the molecule in the UPS spectra is generally accepted as clear evidence of charge transfer. This has been the only direct evidence for the presence of a gap state in photoemission spectroscopy spectra. If no new feature appears and there is minimal change of the rest of the spectrum then it has been generally assumed that there is no significant interaction, charge transfer or chemical reaction at the surface. There is very little change in the UPS spectra but the appearance of gap state is discovered in the IPES spectra. The vacuum level and HOMO position both shift ~ 0.2 eV after only 1 Å of Au deposition yet a gap state appears in the unoccupied energy level where the Fermi level is pinned. (Fig. 2-6) This direct evidence of a gap state appearing in the unoccupied energy levels at the interface of an organic and metal reveals that it is inappropriate to assume that there is no change in the unoccupied electronic structure when there are no significant changes in the UPS or XPS spectra.

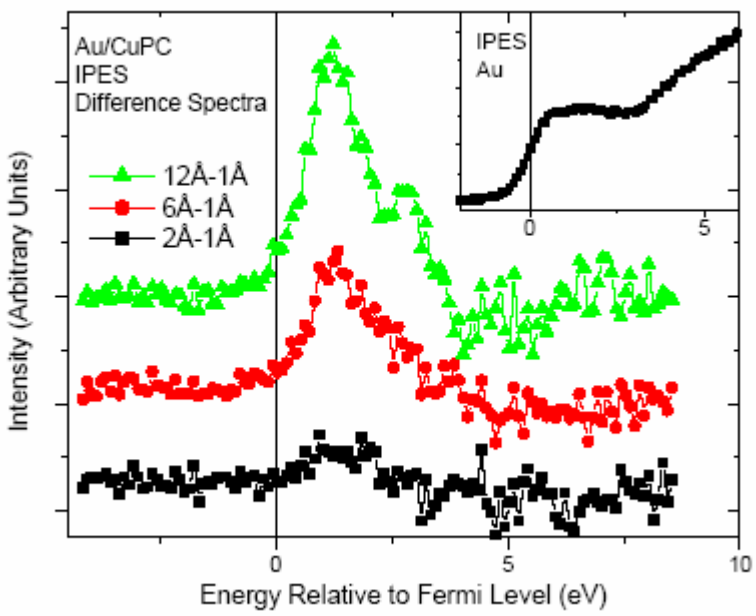

Fig. 2-5 After the initial 1Å of Au the only changes that are seen in the IPES spectra are the growth of new LUMO features. The inset showing the IPES spectra of bulk Au shows that the new features are not simply Au features. (Reprint form [37])

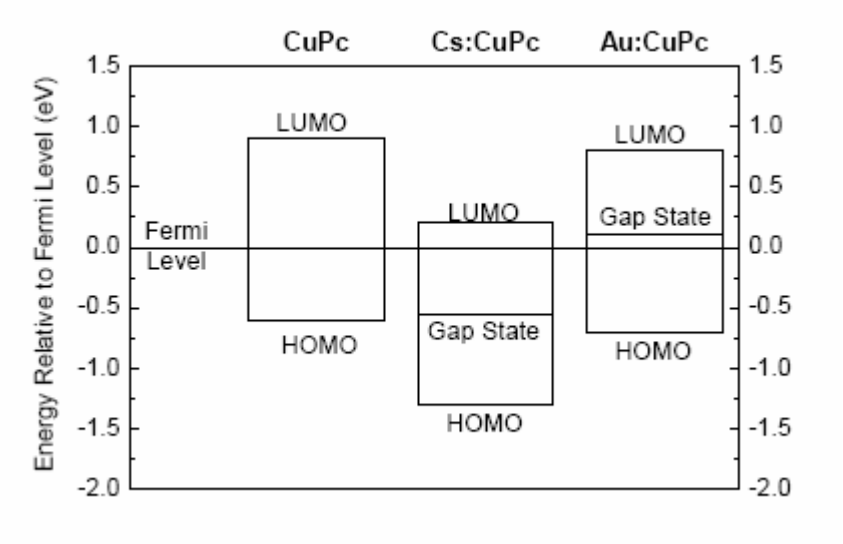

Fig. 2-6. HOMO, LUMO, and Gap State peak onset positions of CuPc, and Au doped CuPc. (Reprint form [37])

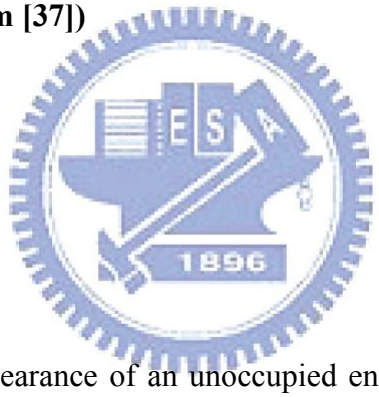

2.3.3 Discussion

From Fig. 2-6, the appearance of an unoccupied energy gap state located ~ 0.8 eV below the LUMO. Therefore, we suggest that the energy diagram of Au/CuPc/pentacene is similar to the energy diagram of Au/CuPc. The hole injected from Au only need to overcome the energy barrier 0.8 eV. This concept shows in Fig. 2-7. In the proceeding chapter, we will demonstrate this concept by analyzing the CuPc modified OTFTs and the pentacene-based diode.

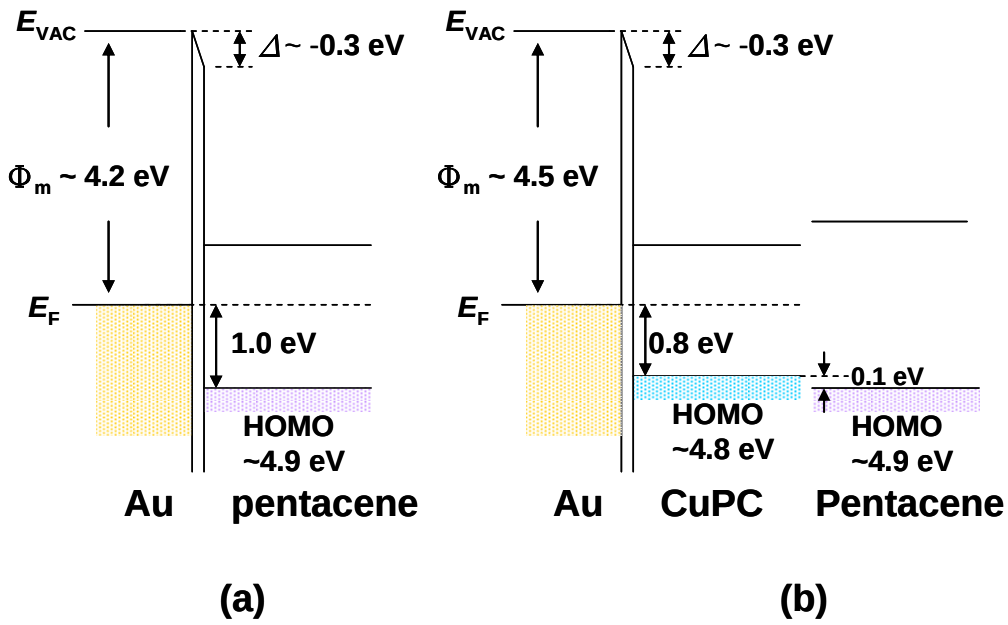

Fig. 2-7 Energy diagram of (a) Au/pentacene (b) Au/CuPc/pentacene.